ACS APPLIED MATERIALS & INTERFACES

Research Article

www.acsami.org

Selective Heterogeneous Catalytic Hydrogenation of Ketone (C═O) to Alcohol (OH) by Magnetite Nanoparticles Following Langmuir–Hinshelwood Kinetic Approach

Muhammad Tariq Shah,[†] Aamna Balouch,*[,†] Kausar Rajar,[†] Sirajuddin,[†] Imdad Ali Brohi,[‡] and Akrajas Ali Umar[§]

[†]National Centre of Excellence in Analytical Chemistry, University of Sindh, Jamshoro 76080, Pakistan

[‡]Centre of Applied Geology, University of Sindh, Jamshoro, 76080, Pakistan

[§]Institute of Microengineering and Nanoelectronics, University Kebangsaan Malaysia, Bangi, 46300, Selangor, Malaysia

ABSTRACT: Magnetite nanoparticles were successfully synthesized and effectively employed as heterogeneous catalyst for hydrogenation of ketone moiety to alcohol moiety by $NaBH_4$ under the microwave radiation process. The improvement was achieved in percent recovery of isopropyl alcohol by varying and optimizing reaction time, power of microwave radiations and amount of catalyst. The catalytic study revealed that acetone would be converted into isopropyl alcohol (IPA) with 99.5% yield in short period of reaction time, using10 μg of magnetite NPs (Fe_3O_4). It was observed that the catalytic hydrogenation reaction, followed second-order of reaction and the Langmuir–Hinshelwood kinetic mechanism, which elucidated that both reactants get adsorb onto the surface of silica coated magnetite nanocatalyst to react. Consequently, the rate-determining step was the surface reaction of acetone and sodium borohydride. The current study revealed an environment friendly conversion of acetone to IPA on the basis of its fast, efficient, and highly economical method of utilization of microwave irradiation process and easy catalyst recovery.

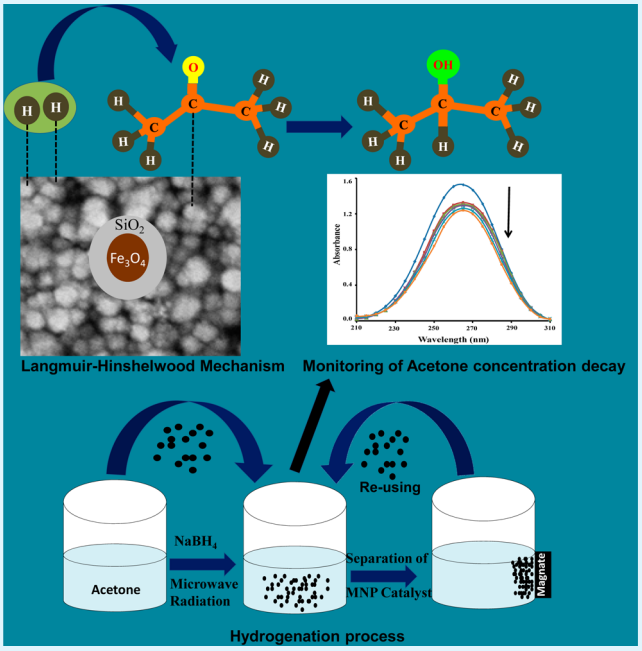

KEYWORDS: *heterogeneous hydrogenation, ketone, alcohol, magnetite nanoparticles, microwave radiation*

1. INTRODUCTION

The reduction of carbonyl compounds is a fundamental transformation in synthetic organic chemistry. Selectivity of hydrogenation reaction is important in both homogeneous and heterogeneous catalytic process. The specific target in hydrogenation process is unsaturated bonds, such as C═C, C═C, or C═O, leaving other unsaturated bonds within the molecule (or in other molecules) unaffected.[1] The selective hydrogenation of organic compound also having different functional groups to be hydrogenated is not an easy goal in synthesis of fine chemical.[2] Catalytic hydrogenation is the most convenient, versatile, and environment friendly and adequate methods for organic synthesis, and the reaction is usually conducted using batch type liquid phase slurry processes and a supported noble metal (Pd, Pt, or Rh) are applied as catalyst.[2−4]

Major advantages of multiphase catalytic reactions using solid catalysts include easy separation of catalysts and products, easy recovery, and catalyst recycling, and relatively mild operating conditions.[5] There are clear economic and environmental incentives to develop heterogeneous catalysts to replace conventional homogeneous catalysts in many industrial processes.[6] Because of easy reduction of carbonyl functional group (C═O) to alcohol functional group (C−OH) the hydrogenation of acetone is economic and environmentally safe process for the production of isopropanol.[7] Since Raney nickel, mixture of metal oxide and supported metal catalyst are reported for the hydrogenation of acetone.[8−15] Though these processes are highly efficient but only when combine with cumene method, which result the toxic and environment unfriendly byproducts such as benzene and cumenehydroperoxide(explosive intermediate) after tedious and multiple-step process. However, high temperature (in

Received: November 8, 2014
Accepted: March 10, 2015
Published: March 10, 2015

DOI: 10.1021/am507778a
ACS Appl. Mater. Interfaces 2015, 7, 6480−6489

many cases can be up to 250 °C), and complicated experimental procedure make these methods costly and time-consuming. Liquid-phase hydrogenation of acetone using Raney nickel catalyst over a broad range of acetone concentration in different solvents, such as *n*-hexane, cyclohexane, methanol, and isopropyl alcohol, is reported by Kishida and Teranishi.[9] The results were effectively inferred by the Langmuir−Hinshelwood (L−H) model with possible adsorption of hydrogen, acetone, and solvent on the similar active sites on surface of catalyst.[9] So far in the literature, no report is available for the use of magnetic NPs to successfully convert acetone to isopropanol. Magnetic NPs will be of high interest because of its good stability and activity for catalytic applications. Such magnetic NPs can be very beneficial to assist an active separation of catalysts.[16]

The immobilized catalysts easily recycled by magnetic decantation and reused many times without losing of activity and enantio selectivity. Core−shell magnetic NPs may facilitate the production of a new type of catalyst. Mostly the shell composed of the catalytically active components, and the magnetic center works as anchor to separate and reprocess the catalyst. If the magnetic core is inherently catalytically active, then it shows both the catalytic and the separation function simultaneously. Thus, 1,6-bis(diphenylphosphino)hexane or polyethylene glycol stabilized iron NPs exhibit high catalytic activity for the reaction of aryl Grignard reagents cross coupled with primary and secondary alkyl halides having b-hydrogen atoms. It is also reported as an efficient and effective catalyst for tandem ring-closing/cross coupling reaction.[17] Such only carbon-supported magnetic catalysts and mesoporous silica decorated with carbon-coated magnetic NPs are proven as highly active and stable in the hydrogenation of octane, and advantageous due to their trouble-free separation simply by applying a magnetic field.[18] Here, we demonstrate tetraethoxysilane modified magnetite NPs as highly efficient, excellent and selective heterogeneous catalyst for the hydrogenation of acetone to isopropanol. The concept of encapsulation of ultrasmall nanostructures within silica is to reduce the aggregation of magnetite nanocatalyst, protect these nanocatalysts from oxidation and to render the catalyst's surface a negative charge (silinol groups). Other reason behind the selection of silica as a coating agent was its porous nature, which ensures the access of reactants molecules to the surface of magnetite nanocatalyst for the reaction.[19,20]

Metals doped and modified magnetite NPs have been widely used as catalysts but for hydrogenation of acetone to isopropanol SiO_2@Fe_3O_4 NPs as catalyst has not been reported yet. Hereby, we demonstrated easy synthesis of SiO_2@Fe_3O_4 nanocatalyst and, a highly efficient and selective production of isopropanol by hydrogenation of acetone. Approximately 99.5% yield of IPA within a short reaction time was achieved. Because of easy preparation, faster hydrogenation process, and heterogeneous catalysis system, which prevent hydrogenation reaction from catalyst contamination the SiO_2@Fe_3O_4 NPs can be applied as an environmental friendly catalyst for the selective production of isopropanol.

2. EXPERIMENTAL SECTION

2.1. Reagents and Apparatus. Analytical grade reagents were used throughout the synthesis and application procedures. Ferrous chloride tetrahydrated ($FeCl_2{\cdot}4H_2O$) and ferric chloride hexahydrated ($FeCl_3{\cdot}6H_2O$) were purchased from sigma-Aldrich Company. NH_4OH, $FeCl_2{\cdot}4H_2O$, $FeCl_3{\cdot}6H_2O$, and deionized water were used to prepare acetone and TEOS aqueous solutions. The glasswares were soaked in 15% (v/v) HNO_3 solution for a single night. Later on, they were washed with copious amount of deionized water and were kept into in an oven at 110 °C for dry.

2.2. Synthetic Procedure for Tetraethoxysilane Modified Magnetite Nanoparticles. Highly efficient magnetite nanocatalyst was synthesized by dissolving appropriate mass of precursor salts, $FeCl_3{\cdot}6H_2O$ and $FeCl_2{\cdot}4H_2O$ to make 2:1 mole ratio solution in 200 mL of deionized water, respectively. The complete dissolution of precursor salts was achieved under vigorous mechanical stirring at 85 °C. Then $NaBH_4$ was added to reduce the precursor ($FeCl_3{\cdot}6H_2O$ and $FeCl_2{\cdot}4H_2O$) and subsequently 25 mL of 30% ammonium hydroxide (NH_4OH) were added rapidly to form large number of nuclei to prevent aggregation of magnetite NPs. The orange color of the solution was changed into black with the addition of (NH_4OH) instantly. The stirring was continued for 15 min after the addition of ammonium hydroxide, final pH of the solution was 13 (data not shown). The magnetite NPs were washed twice with 0.02 M sodium chloride (NaCl) solution. They were washed several times with deionized water and were dried in vacuum oven at 50 °C. After they were dried, particles were stored in deionized water at concentration 40 g/L until further process.

The above synthesized magnetite NPs were coated with tetraethoxysilane (TEOS) to enhance the surface activity of magnetite NPs and maintain the dispersion of the particles in the solution. For achieving this purpose, magnetite NPs were treated as per reported method with 10% TEOS solution and 60 mL of glycerol at pH 4.6.[21] The solution was heated at 80 °C for 90 min under vigorous mechanical stirring. After the solution was cooled to the room temperature, tetraethoxysilane modified magnetite precipitates were at first swab numerous times with ethanol and then three to four times with deionized water. The SiO_2@Fe_3O_4 NPs were separated from water with the help of a magnet through magnetic decantation and dried in vacuum oven at 50 °C for 5 h. The confirmation of particles was done by Fourier transform infrared (FT-IR) microscopy, (Thermo Nicolet 5700) in the transmission mode with a resolution of ±4 cm^{-1}, a wavenumber range of 4000−400 cm^{-1} with a deuterated triglycine sulfate as a detector. The morphology and particle size and shape were characterized by Zeiss Supra 55VP FESEM model of Field emission scanning electron microscopy (FESEM) with 1.0 nm resolution at 30 Kv and Philips CM 12 model of Transmission Electron Microscopy (TEM) with 1.4 to 4 Å varying resolution at 120 kV. The crystal structure was analyzed by Bruker D8 X-ray diffraction (XRD) system with a CuKα and 0.025 deg/s irradiation and scanning rate, respectively.

2.3. Heterogeneous Catalytic Application of Silica-Modified Fe_3O_4 NPs. The evaluation of catalytic efficiency of the magnetite nanostructure was conducted by the hydrogenation of acetone to isopropanol under microwave irradiation. In typical procedure, a 10.0 mL of 0.1 mol L^{-1} aqueous acetone solution was taken in glass vial. Afterword it was placed in Teflon sealed tube and irradiated under microwaves in the absence and presence of SiO_2@Fe_3O_4 nanocatalyst. The solution was continuously irradiated at low power 10% of 1100 W throughout the reaction process. To evaluate the SiO_2@Fe_3O_4 NPs catalytic effect on acetone hydrogenation reaction, UV−visible absorption spectrum was recorded after every 10 s time by taking approximately 4 mL of the solution into a quartz cuvete. The Biochrom Libra S22 UV−visible spectrophotometer was used for absorption measurement of the solution during the progress of hydrogenation reaction.

However, to improve percent yield of isopropyl alcohol, the amount of catalyst, microwave irradiation power and the effect of reaction time on the hydrogenation of acetone were optimized at constant concentration of acetone (0.10 mol L^{-1}) to find optimum values. The same concentration range was also applied in absence of SiO_2@Fe_3O_4 nanocatalyst to evaluate the nature of the acetone hydrogenation to isopropanol reaction.

The production of isopropanol by acetone hydrogenation was confirmed by gas chromatographic analysis. For this purpose, a flame ionization detector (FID) equipped with gas chromatographic

DOI: 10.1021/am507778a
ACS Appl. Mater. Interfaces 2015, 7, 6480−6489

instrument (Agilent 5890 series II) was used. The instrumental conditions are followed as reported in our previous work.[28]

Standard calibration graph of acetone concentration vs absorption was plotted to quantify isopropanol concentration. Graph was plotted in the concentration range of 0.01−0.2 mol L^{-1} and change in absorbance was noted at 265 nm. Further calculations and experimental procedure was conducted as reported by Aamna at.el.[28]

3. RESULTS AND DISCUSSION

Magnetite NPs were successfully prepared by coprecipitation method at ambient laboratory conditions. To confirm the components of SiO_2@ Fe_3O_4 core−shell NPs, the FTIR spectrum analysis were carried out whose results are shown in Figure 1. The peaks in blue and red lines in spectrum show the

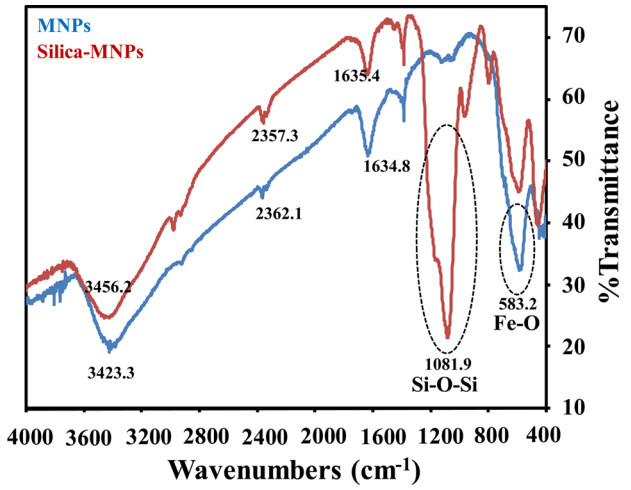

Figure 1. FTIR spectra of magnetite NPs (blue line) and silica-coated magnetite NPs (red line).

result before and after coating the surface of magnetite NPs. The characteristic absorption peak at 583.2 cm^{-1} in spectrum (Blue line) is due to asymmetric stretching of Fe−O bond of magnetite (Fe_3O_4) phase and peaks at 1634.8 and 3423.3 cm^{-1} are attributed to asymmetric stretching vibration of H−O−H bonds of water present in the sample and O−H bond held through hydrogen bonding or physisorption on the surface of magnetite NPs. After silica coating some new peaks appear on the magnetite spectrum (red line). A sharp peak at 1081.9 cm^{-1} and two small peaks at 964.2 and 796.6 cm^{-1} because of the symmetric and asymmetric stretching vibration of Si−O−Si groups, which confirm the successful coating of magnetite NPs surface with silica. The shifting of characteristic peak Fe−O−Fe of magnetite (Blue line) from 583.2 to 591.6 cm^{-1} in the spectrum of SiO_2@Fe_3O_4 (red), also indicate the coating of silica shell on the surface of the magnetite NPs. Silica coating on the surface of magnetite NPs is also confirmed from literature.[22−25]

The surface morphology of magnetite (Fe_3O_4) NPs and tetraethoxysilane (TEOS), modified magnetite (SiO_2@Fe_3O_4) NPs were determined by the field emission scanning electron microscopy (FESEM) as shown in Figure 2 A-D. The images taken at low and high resolution represent bare and silica modified magnetite NPs. From these images, it is clear that most of the particles are spherical and with uniform average size of 5−15 nm. Figure 2A and B shows the formation of magnetite NPs with spherical morphology. Apart from it, some agglomerated form of particles can be seen. Figure 2C and D show the surface of modified particles which are better and smaller in size distribution. It can also be observed that surface of magnetite particles becomes rough after modification with TEOS. These smaller size magnetite NPs with highly rough morphology can be very effective catalyst due to its high electron density and mobility on the surface of the nanoparticles.

TEM analysis was carried out for the further confirmation of the morphology of the bare magnetite and SiO_2@Fe_3O_4 NPs as shown in Figure 3 (A and B). TEM images of bare magnetite in Figure 3A show the spherical magnetite NPs with an average diameter of 10−15 nm. Besides, some of the particles can also be seen with random shapes. Figure 3B shows TEM image of successfully SiO_2@Fe_3O_4 NPs. A clear thin layer of silica indicated in Figure 3B that magnetite is successfully coated. The average diameter of magnetite NPs after silica coating is almost same as bare magnetite nanoparticles. The silica modification produced roughness on the surface of magnetite NPs. These small size particles with high surface area to volume ratio could be promising and very much effective catalyst.

Having done the process TEM and FESEM analysis, the crystallographic evaluation of magnetite and SiO_2@Fe_3O_4 NPs were carried out by X-ray diffraction analysis (XRD), shown in Figure 3C and D. The X-ray diffraction powder pattern of the magnetite NPs in Figure 4C showed 6 peaks [(220), (311), (400), (422), (511), and (440)]. These reflection planes indicate the presence of the inverse spinal cubic structure. This reflection pattern matches 99% with Standard (JCPDS file 19-0629) of magnetite. The XRD data of magnetite was also achieved after coating it with silica. Most of the diffraction peaks arising from bare magnetite NPs could still be detected as shown in Figure 4D. However, an interesting result appeared when an extra peak 29.3° 2θ came into our observation after silica coating. This additional peak was assigned to the (220) plane of magnetite silica phase which was further confirmed from literature by corresponding with JCPDS file 73-0963 of SiO_2@Fe_3O_4 MNPs. The mixed magnetite silica phase was formed at the interface of silica and magnetite during core−shell synthesis of SiO_2@Fe_3O_4NPs.

The further confirmation of the Fe_3O_4 nanostructures was done by energy dispersive X-ray spectroscopic (EDS) analysis. The elemental composition of Fe_3O_4 and SiO_2@Fe_3O_4 NPs is shown in Figure 4A and B. From Figure 4A, it is clear that the EDS spectrum for Fe_3O_4 contains only iron and oxygen elements whereas the presence of iron, oxygen and silicon in spectrum 4B confirms that the synthesized nanostructure is composed of SiO_2@Fe_3O_4 NPs. There are no any other impurity elements present in Fe_3O_4 and SiO_2@Fe_3O_4 NPs. The small carbon peak is due to background carbon adhesive tape.

3.1. Catalytic Application of Silica-Modified Fe_3O_4 NPs. Catalytic activity of silica-modified Fe_3O_4 NPs was checked in acetone hydrogenation reaction to isopropanol under microwave irradiation. The Biochrom Libra S22 UV−visible spectrophotometer was used for absorption spectrum measurement. Change in absorbance spectrum of acetone at 265 nm such as hypochromic effect and hypsochromic effect confirm the hydrogenation. The hypochromic effect (decrease in the absorbance) and hypsochromic effect (blue-shifting) of acetone peak at 265 nm revealed the decrease in concentration of acetone and selective production of isopropanol, under microwave radiation.[15,26]

However, to obtain high percent yield, the amount of catalyst, microwave irradiation power and time for the

DOI: 10.1021/am507778a
ACS Appl. Mater. Interfaces 2015, 7, 6480−6489

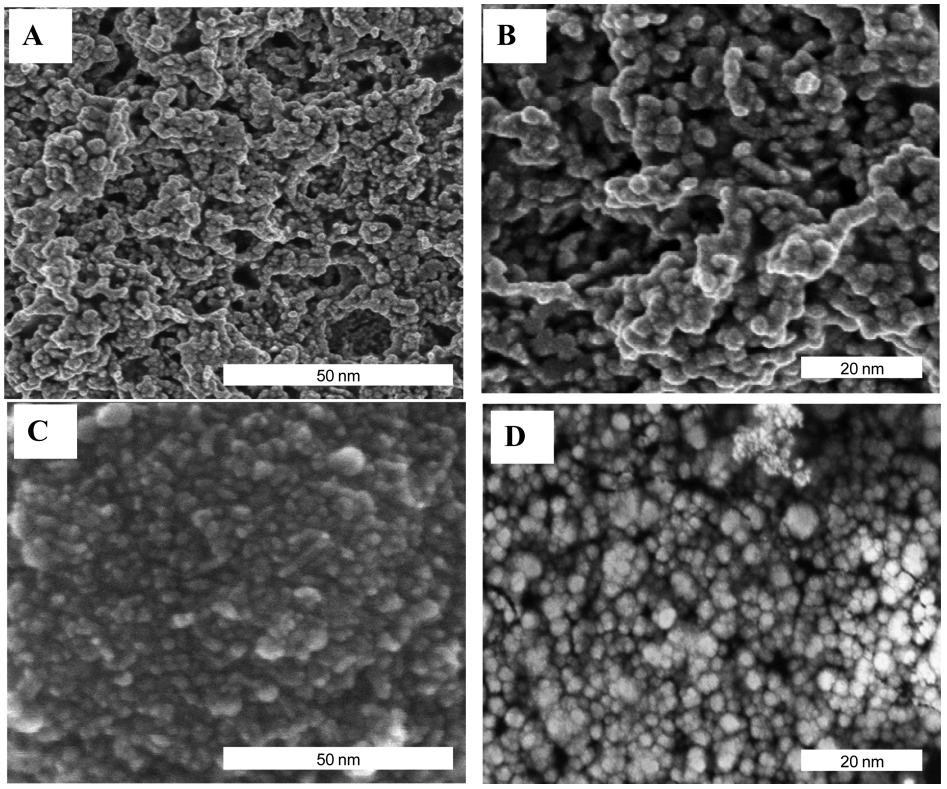

Figure 2. FESEM images (A and B) low and high resolution of magnetite NPs and images (C and D) low and high resolution of silica-coated magnetite NPs.

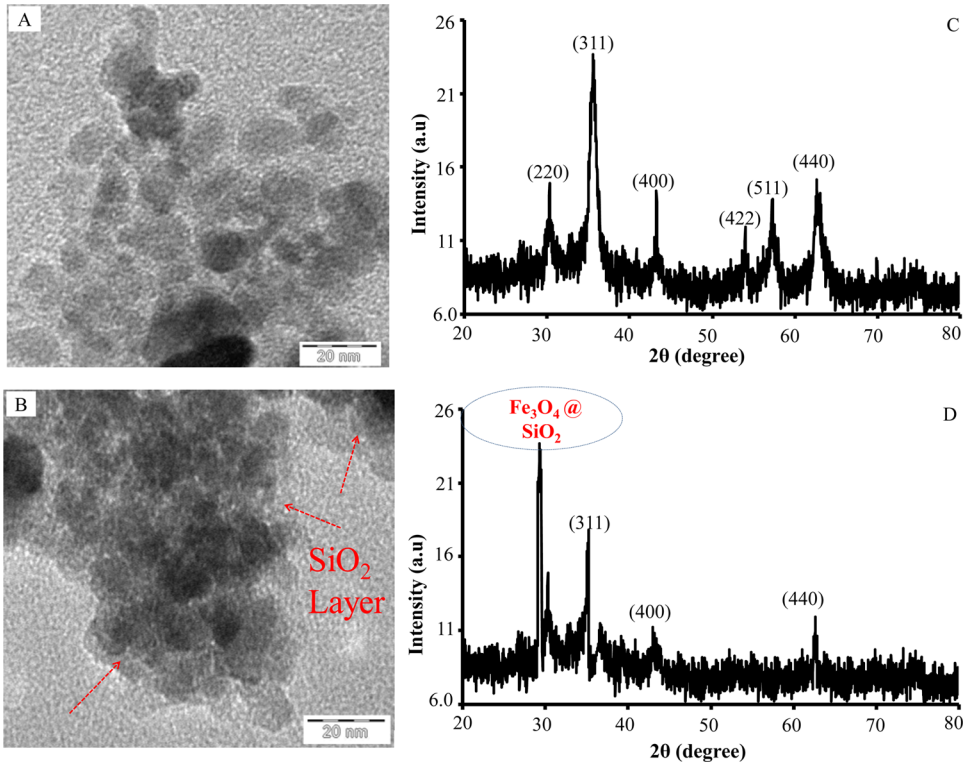

Figure 3. TEM image of magnetite NPs (A) and silica-coated magnetite NPs (B) XRD spectrum of magnetite NPs (C) and silica-coated magnetite NPs (D).

hydrogenation reaction was conducted at fixed concentration of acetone (0.10 mol L^{-1}). The same concentration range was also applied in absence of SiO_2@Fe_3O_4 NPs to evaluate the nature of the conversion of acetone to isopropanol reaction.

DOI: 10.1021/am507778a
ACS Appl. Mater. Interfaces 2015, 7, 6480−6489

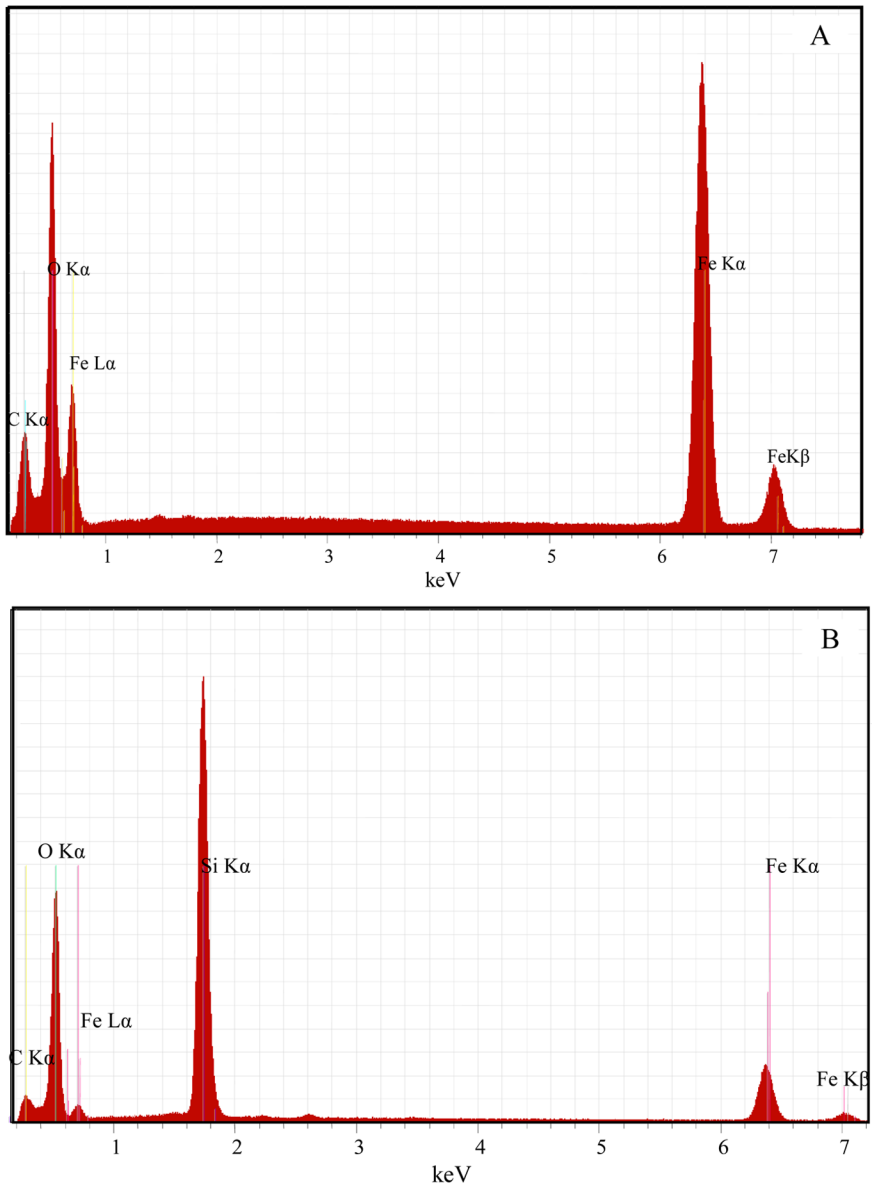

Figure 4. EDS elemental analysis of (A) bare magnetite and (B) silica-coated magnetite particles.

As this process was heterogeneous in nature and easy in operation, the SiO_2@Fe_3O_4 NPs system became a potential alternative for environment friendly and economical in large scale synthesis of isopropyl alcohol. Because of the small size and rough surface of SiO_2@Fe_3O_4 NPs was proved as an effective catalyst for the hydrogenation of acetone to isopropanol in the present system. It could be attributed to silica binding on the surface of magnetite NPs that provided high surface area for adsorption. Silane-modified magnetite (SiO_2@Fe_3O_4) NPs were used as a catalyst in hydrogenation of acetone to IPA. At First, the sodium borohydride and the acetone adsorb on the SiO_2@Fe_3O_4 nanocatalyst surface to form pseudocarbon−catalystbond and pseudo sodium borohydride−catalyst bond.[27] During the reaction SiO_2@Fe_3O_4 NPs activate the carbonyl carbon toward the attack of weak nucleophile ($NaBH_4^-$). The acetone hydrogenation reaction on the surface of SiO_2@Fe_3O_4 NPs catalyst completes in two steps. Initially the hydride ions (H^-) from sodium borohydride attack on the carbonyl carbon atom partially attached to the surface of the catalyst. Then in the second step an electrophile H^+ (protons) from water attack on the electronegative oxygen of carbonyl group of acetone resulting in formation Isopropanol. Schematic representation of reaction mechanism for the hydrogenation of acetone is shown in Scheme 1. Consequently the process ends with the breaking the carbon-catalyst bond which result desorption of the alcohol product from the surface of catalyst. A vacant space is created after desorption of isopropanol molecule from catalyst surface for incoming hydrogen and acetone molecule.[26] This hydrogenation process proved fast, efficient and got completed in 60 s.

The high selectivity of the present method can be attributed to high catalytic activity of SiO_2@Fe_3O_4 NPs with high surface energy, which results in the selective and efficient production of isopropanol.[28] To achieve maximum catalytic efficiency in terms of yield of IPA many factors (microwave radiation power, effect of $NaBH_4$, effect of time, and catalyst dose) were optimized. They produced the results as shown in Figures 5 and 6.

DOI: 10.1021/am507778a
ACS Appl. Mater. Interfaces 2015, 7, 6480−6489

Scheme 1. Proposed Mechanism for Acetone Hydrogenation on Catalyst Surface

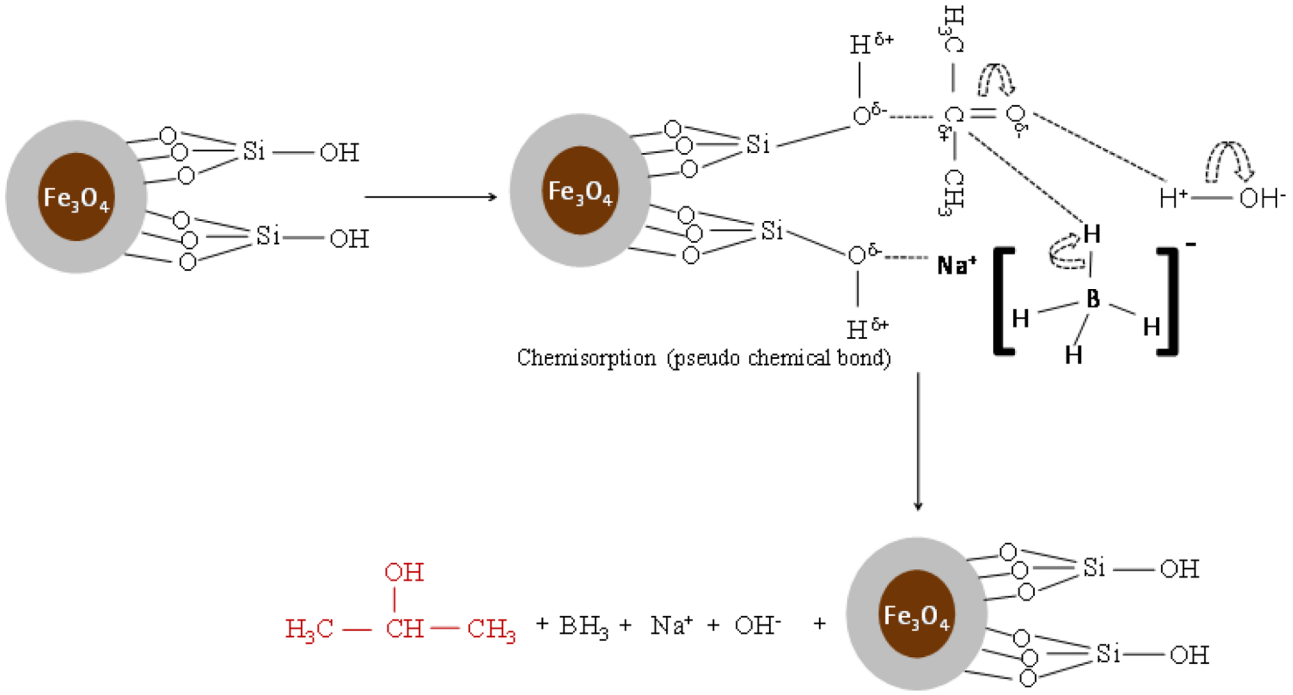

The first parameter we optimized was microwave radiation power by keeping the reaction time constant at the duration of 60 s without using the catalyst and hydrogen source. Variations in the absorption profile of acetone were observed when microwave radiation power was decreased from 100 of 1100 W to 10% as shown in Figure 5A. A noticeable decrease in absorbance was seen as the power of microwave was reduced from 1100 to 110 W. From the absorption trend of acetone we expect formation of isopropanol during the reaction. It is clear from Figure 5B that with increase in power of microwave radiation the percent yield of isopropanol was decreased from 20% to 16%, while keeping the reaction time constant at 60 s. As the irradiation power was increased it caused the rise of the temperature of the system which promoted the formation isobutyl ketone instead of isopropanol.[29] The achieved percent yield of isopropanol was~20 at 110 and 330 W power of microwave radiation. Afterward a small amount (0.5 mM) of sodium borohydride ($NaBH_4$) was used as a source of hydrogen as reported in our pervious paper.[28] The maximum time was optimized to convert acetone to IPA under 110 W of microwave radiation. Same is reported by Tomin et al. that water can also act as hydrogen source to proceed hydrogenation of acetone to isopropanol.[30] For this purpose, a glass vial containing acetone solution was placed in sealed Teflon tube, which increased the pressure during the reaction after microwave irradiation. Increase in pressure causes the splitting of water molecule, which provides hydrogen in the system. Therefore, we focused more on the power of microwave radiation along with low concentration of $NaBH_4$ result reported in Figure 5C and D.

Moreover, when no further decrease in absorption of acetone peak was observed it showed hydrogenation process was ceased in the system. Subsequently SiO_2@Fe_3O_4 NPs were introduced to check its catalytic properties. Hence, to study the catalytic effect for hydrogenation of acetone to isopropanol, 0.1 M acetone concentration had been selected and different doses of catalyst were added at constant microwave radiations, that is, 110 W as shown in Figure 6A and B. The catalyst dose was important parameter that could affect the process of hydrogenation/reduction of acetone to isopropanol. The experiment was carried out by changing the amount of catalyst keeping other parameter constant, that is, power of microwave radiation (110 W), time (20 s), and concentration of acetone (0.1 M). A significant decrease was observed in the acetone peak by increasing the dose of catalyst from 5 to 100 μg as shown in Figure 6A, a typical UV−visible spectra of acetone at varying amount of catalyst at 20 s reaction time. After calculation the 53% yield of IPA was achieved using 100 μg SiO_2 coated magnetite nanocatalyst. Later on the % yield of IPA at different dose of catalyst with respect to time was checked. The result revealed that the use of 5 μg nanocatalyst only produced maximum 50% IPA at 100 s reaction time until hydrogenation process was ceased. The results in Figure 6B showed that the % yield of IPA was exponentially increased with respect to catalyst dose (10−100 μg) and also the rate of reaction was increased. The maximum 99% yield of IPA obtained at reaction time 60, 50, and 40 s as the dose of catalyst was increased from 10 to 100 μg, respectively. After 60 s of the reaction time, the trend of decrease in % yield revealed from Figure 6B that increase in irradiation time hindered the conversion of acetone to isopropanol. It might be attributed to a rise in the temperature. Also the reaction phenomenon supported the controlling mechanism which was the surface reaction on pore wall and at higher catalyst loading the increased in rate was not significant due to high rate of mass transfer.[31] This facile heterogeneous catalytic method provided easy removal technique for the catalyst from the reaction vial by using permanent magnet. After, it was washed with copious amount of deionized water and was reused for the next reaction in fresh acetone solution. The reusability data showed the 61%, 44%, and 35% yield at second, third and fourth time application of catalyst. It revealed that % yield of IPA was gradually decreased and after third time the use of catalyst and the active sites of catalyst were blocked or exhausted that provided no more catalytic effects as shown in

DOI: 10.1021/am507778a
ACS Appl. Mater. Interfaces 2015, 7, 6480−6489

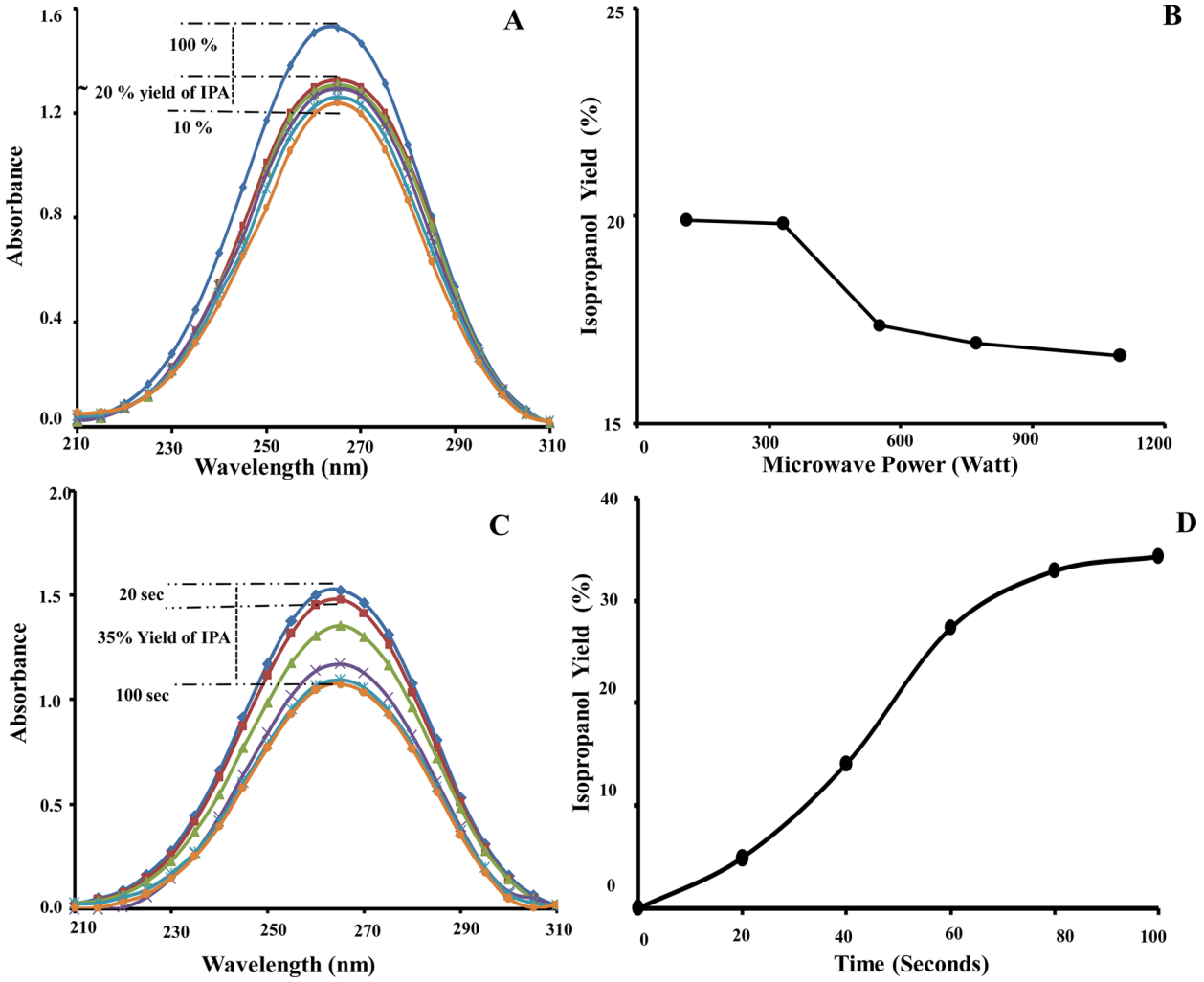

Figure 5. Acetone concentration decay UV-spectrum with respect to microwave power (A), % yield of isopropanol with respect to microwave power (B), acetone concentration decay UV-spectrum with respect to time at $NaBH_4$ (0.5 mM) and 110 W(C), and % yield of isopropanol with respect to time at $NaBH_4$ (0.5 mM) and 110 W (D).

(Figure 6C). Furthermore, the kinetics study was conducted using 10 μg of nanocatalyst as optimized dose at 60 s reaction time. For comparing purpose the bare magnetite nanoparticles were also investigated as heterogeneous catalyst by applying the same experimental protocol as did for SiO_2@Fe_3O_4 (Figure 6D). By using 5 to 100 μg of bare magnetite nanoparticles we observed maximum 41% yield of isopropanol which is about 12% less than SiO_2@Fe_3O_4 NPs. Also catalytic activity of bare magnetite NPs became considerably low in second time use, which probably due to agglomeration of bare magnetite nanoparticles in water system.

3.2. Investigation of Kinetics and Mechanism Reaction. To find out the kinetics rate/order of reaction and type of reaction either physisorption or chemisorptions, we applied 2 models namely Lagergren pseudo-first-order and pseudo-second-order. Lagergren pseudo-first-order and pseudo-second-order kinetics models were used to fit in the experimental data to study the kinetics of heterogeneous catalytic conversion of acetone to isopropanol.

Lagergren first-order model express as eq 3

$$\ln(q_e - q_t) = \ln q_e - \frac{k_1 t}{2.303} \quad (2)$$

where q_t and q_e are the amount of educts (mg g^{-1}) at time t and at equilibrium, k_1 is the rate constant of the pseudo-first-order process (min^{-1}). Straight line plots of $\ln(q_e - q_t)$ against t were used to determine the rate constant k_1, and adsorption capacity (Figure 7A). From results it was concluded that heterogeneous catalytic process on magnetite did not follow pseudo-first-order kinetics because the pseudo-first-order model data did not fall on the straight line.

The equation used to express pseudo-second-order

$$\frac{t}{q_t} \frac{1}{k_2 q_e^2} \frac{t}{q_e} \quad (3)$$

$$h = k q_e^2 \quad (4)$$

where h (mg $g^{-1}min^{-1}$) is the initial hydrogenation rate as t and k_2 is the rate constant of pseudo-second-order hydrogenation (g mg^{-1} min^{-1}). The plot of t/q_t versus t was constructed to evaluate pseudo-second-order model (Figure 7B). The graph showed good straight lines with R^2 = 0.990 as compared to the plot of pseudo-first-order, where the value of q_e, k, and h = 0.1255 mg/g, 0.292 g/mg/s, and 0.0046 mg/g/s were determined from the slope and intercept of the plot, respectively.

DOI: 10.1021/am507778a
ACS Appl. Mater. Interfaces 2015, 7, 6480−6489

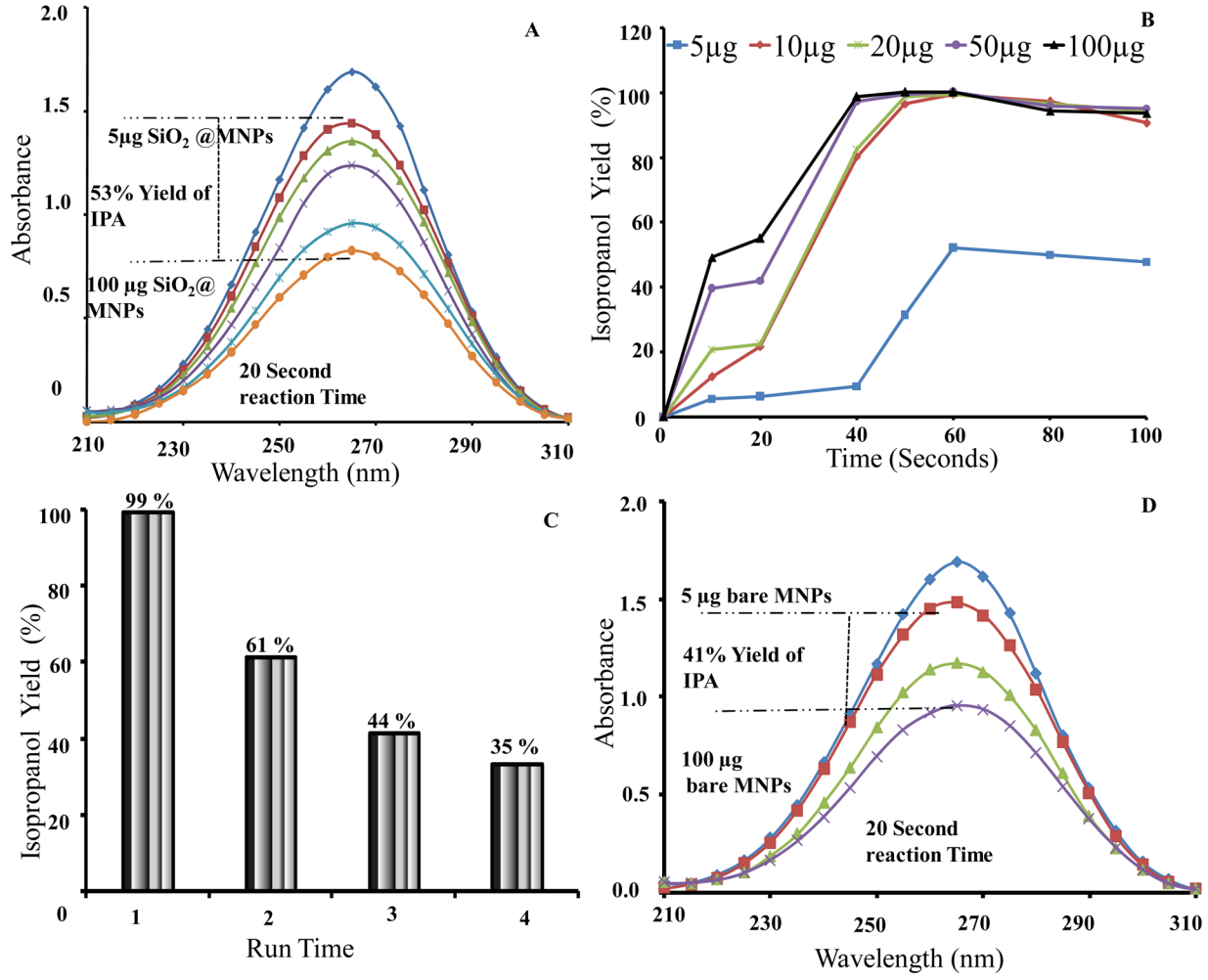

Figure 6. Acetone concentration decay spectrum for the experiments performed with chemical mixtures of silica-coated magnetite with acetone within 20 s reaction time (A), % yield of isopropanol with respect to magnetite nanocatalyst dose and time (B), reusability of magnetite nanocatalyst (C), and acetone concentration decay spectrum bare magnetite nanoparticles (D).

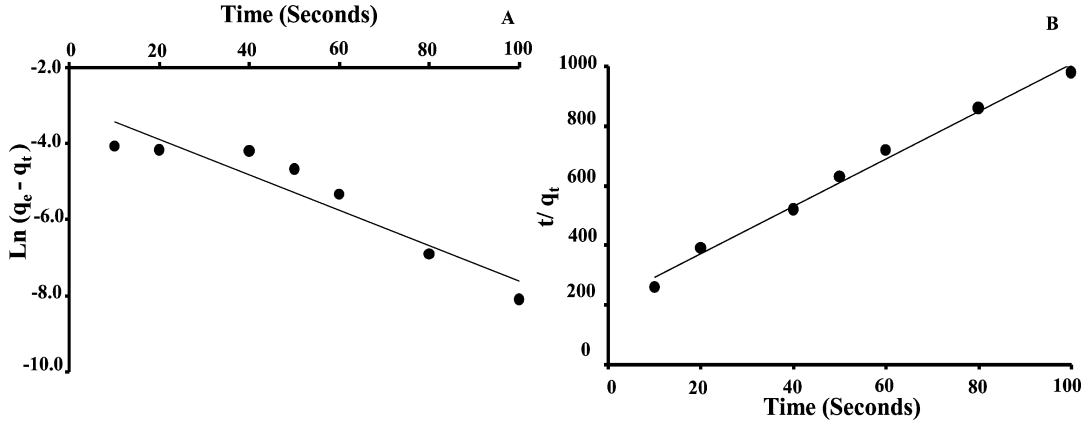

Figure 7. Pseudo-first-order of reaction (A) and pseudo-second-order of reaction (B).

Additionally, experimental qe_{exp} value is in a good accordance with the calculated equilibrium catalytic capacity qe_{cal}. Therefore, it is possible to suggest that the hydrogenation of acetone by magnetite NPs followed pseudo-second-order reaction, which postulates that hydrogenation reaction basically following chemisorption phenomenon. It may be the rate-limiting step. In chemisorptions, the acetone and hydrogen molecule attached to the $SiO_2@Fe_3O_4$ surface and make pseudo-bond and try to find active sites that may increase their coordination number with the surface.

Therefore, it was concluded that the pseudo-second-order kinetic model provided a better correlation for the adsorption of reactants molecule on $SiO_2@Fe_3O_4$ NPs at different initial concentration compared to the pseudo-first-order model.

DOI: 10.1021/am507778a
ACS Appl. Mater. Interfaces 2015, 7, 6480−6489

For the determination of mechanism two major reaction modes are promising for a surface reaction. Eley–Rideal model, which determines that during reaction one of the reactant is adsorbed onto the surface of catalyst/adsorbent and reacts with the other reactant present in solution.[32] Second mechanism is the Langmuir–Hinshelwood, which is the most commonly used kinetic model for heterogeneous catalytic processes. Langmuir–Hinshelwood mechanism is followed when both reacting species are simultaneously adsorbed onto the catalyst/adsorbent surface then to react with each other. In this model rate-determining step is the surface reaction. Consequently, the adsorption of the reactants to the catalyst surface and the dispersal of the products from the catalyst surface should be quicker than the reaction step itself.[32,33]

In typical reaction procedure for Langmuir–Hinshelwood a wide concentration regime of acetone (0.01–0.1 mol L^{-}) was tested with a constant concentration of sodium borohydride (0.05 mol L^{-1}) Figure 8A. Second, for Eley–Rideal model, various concentrations of sodium borohydride were investigated with constant concentrations of acetone Figure 8B.

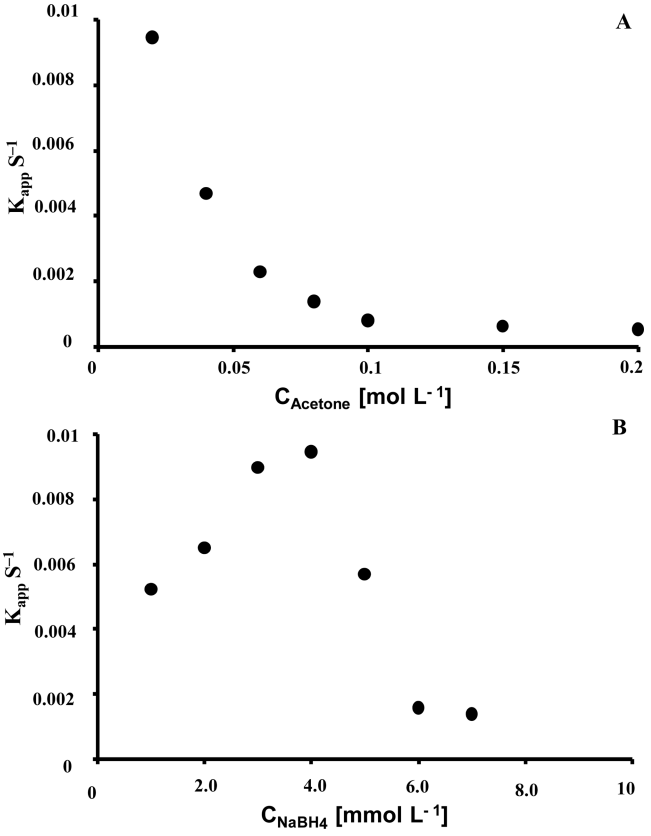

Figure 8. Apparent rate constant K_{app} versus concentration of acetone (A) and apparent rate constant K_{app} versus concentration of $NaBH_4$ (B).

Figure 8 showed the rate constant dependence on the concentration of acetone and sodium borohydride and the rate constant was decreasing with an increasing concentration of acetone it became evident that this reaction followed a Langmuir–Hinshelwood mechanism. Because of adsorption of reactants, borohydride, and acetone, onto the surface of magnetite NPs, in the rate-determining step, reaction starts between the surface hydrogen and the acetone and after the completion of reaction the product (isopropanol) desorbs from the surface of the catalyst producing free active sites on the surface of catalyst again. Furthermore, the diffusion of the educts to the nanocatalyst surface and establishment of equilibrium during the adsorption/desorption process is expected to be rapid. Schematic representation of reaction mechanism for the hydrogenation of acetone is presented in Scheme 1.

4. CONCLUSION

The magnetites NPs were successfully modified with tetraethylorthosilicate (TEOS) to stabilize the magnetite NPs by making core–shell and to prevent the magnetite surface from oxidation. The synthesized SiO_2@Fe_3O_4 NPs were responsible for the efficient catalytic hydrogenation reaction regarding the 99.5% conversion of acetone to isopropyl alcohol (IPA) in the presence of microwave radiations within 60 s of reaction time. The present system is the highly selective for isopropanol it does not show byproduct. Active sites located on the surface of SiO_2@Fe_3O_4 NPs were responsible for the quick adsorption of acetone and hydrogen on the surface of the catalyst resulting in a short time equilibrium establishment for the reaction. Moreover, the separation process was quick, simple and convenient because of magnetic separation. Hereafter, we infer that the synthesized SiO_2@Fe_3O_4 NPs are green catalyst due to easily recoverable and reusable by applying magnetic field. SiO_2@Fe_3O_4 nanocatalyst could be recommended for hydrogenation of organic compounds with low molecular weight. Present approach is very simple, easy, economical, and greener method for the production of isopropanol and could be used for fuel cell.

AUTHOR INFORMATION

Corresponding Author

*E-mail: aamna_balouch@yahoo.com.

Notes

The authors declare no competing financial interest.

ABBREVIATIONS

TEOS, tetraethoxysilane/tetraethyl orthosilicate; NPs, nanoparticles; IPA, isopropyl alcohol

REFERENCES

(1) Silvestre-Albero, J.; Rupprechter, G.; Freund, H.-J. Atmospheric Pressure Studies of Selective 1,3-Butadiene Hydrogenation on Pd Single Crystals: Effect of CO Addition. *J. Catal.* **2005**, *235*, 52–59.

(2) Domínguez-Quintero, O.; Martínez, S.; Henríquez, Y.; D'Ornelas, L.; Krentzien, H.; Osuna, J. Silica-Supported Palladium Nanoparticles Show Remarkable Hydrogenation Catalytic Activity. *J. Mol. Catal. A: Chem.* **2003**, *197*, 185–191.

(3) Guczi, L.; Horváth, A.; Beck, A.; Sárkány, A. 75 Controlling Metal Particle Size in Preparation of Pd/SiO_2 Catalysts. *Stud. Surf. Sci. Catal.* **2003**, *145*, 351–354.

(4) Stanger, K. J.; Tang, Y.; Anderegg, J.; Angelici, R. J. Arene Hydrogenation Using Supported Rhodium Metal Catalysts Prepared from $[Rh(COD)H]_4$, $[Rh(COD)_2]^+BF_4^-$, and $[Rh(COD)Cl]_2$ Adsorbed on SiO_2 and Pd–SiO_2. *J. Mol. Catal. A: Chem.* **2003**, *202*, 147–161.

(5) Bhanage, B. M.; Arai, M. Catalyst Product Separation Techniques in Heck Reaction. *Catal. Rev.: Sci. Eng.* **2001**, *43*, 315–344.

(6) Salvapati, G.; Ramanamurty, K.; Janardanarao, M. Selective Catalytic Self-Condensation of Acetone. *J. Mol. Catal.* **1989**, *54*, 9–30.

(7) Sumodjo, P. T. A.; da Silva, E. J.; Rabockai, T. Electrosorption of Hydroxylated Compounds: A Comparative Study of Molecules with

DOI: 10.1021/am507778a
ACS Appl. Mater. Interfaces 2015, 7, 6480–6489

Three Carbon Atoms. *J. Electroanal. Chem. Interfacial Electrochem.* **1989**, *271*, 305−317.
(8) Jing, S.; Wang, Z.; Zhu, W.; Guan, J.; Wang, G. Oxidation of Cyclohexane with Hydrogen Peroxide Catalyzed by Dawson-Type Vanadium-Substituted Heteropolyacids. *React. Kinet. Catal. Lett.* **2006**, *89*, 55−61.
(9) Kishida, S.; Teranishi, S. Kinetics of Liquid-Phase Hydrogenation of Acetone Over Raney Nickel Catalyst. *J. Catal.* **1968**, *12*, 90−96.
(10) Kim, T. G.; Yeo, Y. K.; Song, H. K. Chemical Heat Pump Based on Dehydrogenation and Hydrogenation of Isopropanol and Acetone. *Int. J. Energy. Res.* **1992**, *16*, 897−916.
(11) Lemcoff, N. Liquid Phase Catalytic Hydrogenation of Acetone. *J. Catal.* **1977**, *46*, 356−364.
(12) Sen, B.; Vannice, M. A. Metal-Support Effects on Acetone Hydrogenation Over Platinum Catalysts. *J. Catal.* **1988**, *113* (1), 52−71.
(13) Gandia, L.; Diaz, A.; Montes, M. Selectivity in the High-Temperature Hydrogenation of Acetone with Silica-Supported Nickel and Cobalt Catalysts. *J. Catal.* **1995**, *157*, 461−471.
(14) Gandia, L. M.; Montes, M. Effect of the Reduction Temperature on the Selectivity of the High Temperature Reaction of Acetone and Hydrogen Over Alumina and Titania Supported Nickel and Cobalt Catalysts. *J. Mol. Catal.* **1994**, *94*, 347−367.
(15) Narayanan, S.; Unnikrishnan, R. Acetone Hydrogenation Over Co-precipitated Ni/Al_2O_3, Co/Al_2O_3 and Fe/Al_2O_3 catalysts. *J. Chem. Soc., Faraday Trans.* **1998**, *94*, 1123−1128.
(16) Lu, A. H.; Salabas, E. L.; Schüth, F. Magnetic Nanoparticles: Synthesis, Protection, Functionalization, and Application. *Angew. Chem., Int. Ed.* **2007**, *46*, 1222−1244.
(17) Bedford, R. B.; Betham, M.; Bruce, D. W.; Davis, S. A.; Frost, R. M.; Hird, M. Iron Nanoparticles in the Coupling of Alkyl Halides with Aryl Grignard Reagents. *Chem. Commun.* **2006**, *13*, 1398−1400.
(18) Lu, A.-H.; Li, W.-C.; Kiefer, A.; Schmidt, W.; Bill, E.; Fink, G.; Schüth, F. Fabrication of Magnetically Separable Mesostructured Silica with an Open Pore System. *J. Am. Chem. Soc.* **2004**, *126*, 8616−8617.
(19) Mondal, S.; Samanta, A.; Dhar, B. B.; Devi, R. N. Encapsulation of Ultra Small Metal Clusters in Silica: Evolution of the Concept of Nanoreactors and the Case of Ag−Pd@SiO_2 Alloy Catalyst. *Catal. Today* **2014**, DOI: 10.1016/j.cattod.2014.11.006.
(20) Ferroudj, N.; Nzimoto, J.; Davidson, A.; Talbot, D.; Briot, E.; Dupuis, V.; Bée, A.; Medjram, M. S.; Abramson, S. Maghemite Nanoparticles and Maghemite/Silica Nanocomposite Microspheres as Magnetic Fenton Catalysts for the Removal of Water Pollutants. *Appl. Catal. B: Environ.* **2013**, *136−137* (0), 9−18.
(21) Shishehbore, M. R.; Afkhami, A.; Bagheri, H. Salicylic Acid Functionalized Silica-Coated Magnetite Nanoparticles for Solid Phase Extraction and Preconcentration of Some Heavy Metal Ions from various Real Samples. *Chem. Cent. J.* **2011**, *5*, 41−50.
(22) Chen, J. P.; Yang, P. C.; Ma, Y. H.; Tu, S. J.; Lu, Y. J. Targeted Delivery of Tissue Plasminogen Activator by Binding to Silica-Coated Magnetic Nanoparticle. *Int. J. Nanomed.* **2012**, *7*, 5137−5149.
(23) Luong, N. H.; Phu, N. D.; Hai, N. H.; Thuy, N. T. D. Surface Modification of SiO_2-Coated FePt Nanoparticles with Amino Groups. *e-J. Surf. Sci. Nanotechnol.* **2011**, *9*, 536−538.
(24) Quy, D. V.; Hieu, N. M.; Tra, P. T.; Nam, N. H.; Hai, N. H.; Son, N. T.; Nghia, P. T.; Anh, N. T. V; Hong, T. T.; Luong, N. H. Synthesis of Silica-Coated Magnetic Nanoparticles and Application in the Detection of Pathogenic Viruses. *J. Nanomater.* **2013**, 1−6.
(25) Madrakian, T.; Afkhami, A.; Zolfigol, M. A.; Ahmadi, M.; Koukabi, N. Application of Modified Silica Coated Magnetite Nanoparticles for Removal of Iodine from Water Samples. *Nano-Micro Lett.* **2012**, *4*, 57−63.
(26) Guella, G.; Zanchetta, C.; Patton, B.; Miotello, A. New Insights on the Mechanism of Palladium-Catalyzed Hydrolysis of Sodium Borohydride from ^{11}B NMR Measurements. *J. Phys. Chem. B* **2006**, *110*, 17024−17033.
(27) Shokrolahi, A.; Zali, A.; Keshavarz, M. H. Reductive Amination of Aldehydes and Ketones by $NaBH_4$ Using Carbon-Based Solid Acid (CBSA) as Catalyst. *Green Chem. Lett. Rev.* **2011**, *4*, 195−203.
(28) Balouch, A.; Ali Umar, A.; Shah, A. A.; Mat Salleh, M.; Oyama, M. Efficient Heterogeneous Catalytic Hydrogenation of Acetone to Isopropanol on Semihollow and Porous Palladium Nanocatalyst. *ACS Appl. Mater. Interfaces* **2013**, *5*, 9843−9849.
(29) Djakovitch, L.; Koehler, K. Heck Reaction Catalyzed by Pd-Modified Zeolites. *J. Am. Chem. Soc.* **2001**, *123*, 5990−5999.
(30) Tomin, A.; Lazarev, A.; Bere, M. P.; Redjeb, H.; Török, B. Selective Reduction of Ketones Using Water as a Hydrogen Source Under High Hydrostatic Pressure. *Org. Biomol. Chem.* **2012**, *10*, 7321−7326.
(31) Yadav, G.; Thathagar, M. Esterification of Maleic Acid with Ethanol Over Cation Exchange Resin Catalysts. *React. Funct. Polym.* **2002**, *52*, 99−110.
(32) Hu, A.; Yee, G. T.; Lin, W. Magnetically Recoverable Chiral Catalysts Immobilized on Magnetite Nanoparticles for Asymmetric Hydrogenation of Aromatic Ketones. *J. Am. Chem. Soc.* **2005**, *127*, 12486−12487.
(33) Wunder, S. Synthesis, Characterization and Catalytic Activity of Immobilized Metallic Nanoparticles. Thesis, Mathematisch-Naturwissenschaftliche Fakultät I, Berlin, Germany, 2013.

DOI: 10.1021/am507778a
ACS Appl. Mater. Interfaces 2015, 7, 6480−6489